

# Low Complexity Hybrid Precoding and Diversity Combining Based on Spatial Lobes Division for Millimeter Wave MIMO Systems

Yun Chen, Da Chen, Yuan Tian, and Tao Jiang

## Abstract

In this paper, we focus on the design of low complexity hybrid analog/digital precoding and diversity combining in the millimeter wave multiple-input multiple-output (MIMO) systems. Firstly, by exploiting the sparseness property of the millimeter wave in the angular domain, we propose a spatial lobes division (SLD) to group the total paths of the millimeter wave channel into several spatial lobes, where the paths in each spatial lobe form a low-rank sub-channel matrix. Secondly, based on the SLD operation, we propose a low complexity hybrid precoding scheme, named HYP-SLD. Specifically, for each low-rank sub-channel matrix, we formulate the hybrid precoding design as a sparse reconstruction problem, and decouple the design of the analog and digital precoding matrices to obtain the near-optimal solution. Simulation results demonstrate that, the proposed HYP-SLD scheme reduces by 99% the complexity of the classic orthogonal matching pursuit (OMP) scheme, and achieves similar spectral efficiency and bit error rate (BER) performances compared with the fully digital precoding scheme. Finally, we further propose a maximum ratio combining (MRC) based diversity combining scheme, named HYP-SLD-MRC, to improve the BER performance. Simulation results also show that, the BER performance of the proposed HYP-SLD-MRC scheme outperforms the fully digital precoding scheme.

## Index Terms

Millimeter wave communication, spatial lobe, hybrid precoding, low complexity, diversity combining.

Y. Chen, D. Chen, Y. Tian, and T. Jiang are with School of Electronic Information and Communications, Huazhong University of Science and Technology, Wuhan 430074, China (e-mail: chen\_yun@hust.edu.cn; chenda@hust.edu.cn; yuan\_tian@hust.edu.cn; tao.jiang@ieee.org).

## I. INTRODUCTION

Millimeter wave communication is one of the most important technologies for the next generation mobile communications [1]. Due to the abundant spectrum resources and large bandwidth, millimeter wave could deliver high data rates and has been used in many fields. For example, the 60 GHz millimeter wave has been successfully applied in personal area network (PAN) [2] and wireless local area network (WLAN) [3], which use about 2 GHz of bandwidth and could provide data rates up to 6 Gbps [4]. However, owing to the high carrier frequency, millimeter wave signals experience severe path loss compared to signals in current cellular band (3G or LTE) [?], which makes millimeter wave face many challenges when applied to the cellular network. Fortunately, the beamforming (precoding) technology in MIMO systems, which will be widely employed in the 5G communication, could form very high precoding gains to compensate for the high path loss of millimeter wave [6].

For millimeter wave MIMO systems, there are three main candidate precoding schemes, i.e., fully digital precoding, analog precoding and hybrid precoding. The fully digital precoding is widely employed in the classic MIMO communication system, which demands radio frequency (RF) chains comparable in number to the antennas [7], [8]. Though multiple data streams could be transmitted simultaneously, the high power consumption of these RF chains makes the fully digital precoding impractical for the millimeter wave MIMO system [9]. In the analog precoding architecture, all the antennas share a single RF chain [10]. Using the phase shifters, analog precoding could obtain high precoding gains with low power consumption, whereas the number of data streams that could be transmitted is limited by the single RF chain. The hybrid precoding was proposed in [11]–[14], where a high-dimensional analog precoder is followed by a low-dimensional digital precoder. Between the analog and digital precoders, the number of the RF chains is much less than the number of antennas. Hybrid precoding could overcome the high power consumption problem for the digital precoding and the disadvantage of limited data streams for the analog precoding. Therefore, the hybrid precoding structure is more attractive to millimeter wave MIMO systems which are equipped with large antenna arrays.

There are many papers devote to the design of the hybrid precoding for millimeter wave MIMO systems [13], [15]–[19]. The hybrid precoding architecture was first proposed for the millimeter wave communications in [13]. According to the sparse structure of the millimeter wave channel, a sparse reconstruction problem was modeled and an orthogonal matching pursuit

(OMP) algorithm was utilized to design a low hardware-complexity precoding solution. Though the OMP scheme could achieve similar performance with the fully digital precoder, it has a major limitation, i.e., the calculation of the unconstrained fully digital precoding matrix requires singular value decomposition (SVD) of the high dimensional millimeter wave channel matrix and there are inverse operations of high dimensional matrices, which dramatically increases the computational complexity. Therefore, most of the recent hybrid precoding literatures focus on reducing the complexity of the hybrid precoding based on [13]. In [15], the authors proposed four methods to achieve different tradeoffs between the performance and complexity for single user hybrid precoding with full channel state information (CSI) system. In [16], [17], the array-of-subarrays architecture was considered to reduce the computing complexity in which each RF chain is only collected with partial antennas. In [18], a parallel-index-selection matrix-inversion-bypass based algorithm was proposed to design low complexity hybrid precoder. In [19], the beamspace schemes were also proposed to obtain low-complexity hybrid precoding matrices, which transformed high-dimensional matrix operations into low-dimensional beamspace matrix operations. The lens antenna array is another effective low complexity hybrid precoding implementation where the analog part is realized by electromagnetic lens. In the lens antennas array, the analog precoding matrices could be simply obtained by selecting the sub-sets of the antennas [20], [21].

To the best of our knowledge, all the above hybrid precoding methods were based on the clustered channel model and did not fully utilize the sparseness property in angular domain of the millimeter wave. According to [22]–[24], the angles of the arrive/departure (AOAs/AODs) of the paths in the millimeter wave channel could be grouped in several separated spatial lobes (SLs). For paths in different spatial lobes, their AOAs/AODs are sufficiently separable, while the AOAs/AODs of the paths in one spatial lobe are relatively close. This sparseness property in the angular domain leads to the possibility to divide the millimeter wave channel orthogonally, which could be utilized to reduce the complexity of the hybrid precoding and improve the system performance.

In this paper, we propose a low complexity hybrid precoding scheme and a diversity combining scheme for the single user millimeter wave MIMO system. By exploiting the sparseness property in angular domain of the millimeter wave, we firstly carry out a spatial lobes division (SLD) operation to group the total paths into several spatial lobes. SLD operation reconstructs the clustered millimeter wave channel into equivalent spatial lobes channel which consists of several

orthogonal sub-channels. Then, based on the SLD operation, we propose a low complexity hybrid precoding scheme, named HYP-SLD, which formulates the hybrid precoding design as a sparse reconstruction problem. For each sub-channel, the HYP-SLD scheme provides a decoupling solution to the design of the analog and digital precoding matrices. Finally, we further propose a maximum ratio combining (MRC) based diversity combining scheme, named HYP-SLD-MRC. For data streams in each sub-channel, the HYP-SLD-MRC scheme sets the corresponding signal-to-noise ratios (SNR) as the weights and adds these data streams together. The main contributions of this paper are summarized as follows.

- We fully utilize the sparseness property in the angular domain of the millimeter wave to design the low complexity hybrid precoding scheme. The complexity of the proposed HYP-SLD scheme is proportional to the number of paths in one spatial lobe (sub-channel). Compared with the OMP scheme, the reduction of complexity is more than 99% for general system parameters.
- Through a simple linear summation operation, the proposed HYP-SLD-MRC scheme maximizes the output SNR for each sub-channel. Therefore, the BER performance is greatly improved compared with the fully digital precoding scheme. Moreover, since the HYP-SLD-MRC scheme deals with each sub-channel rather than the total signals for the millimeter wave MIMO systems, the multiplexing gains could also be obtained.

Simulation results demonstrate that the proposed HYP-SLD achieves similar spectral efficiency and BER performances compared with the fully digital precoding scheme. Moreover, the BER performance of the proposed HYP-SLD-MRC outperforms the fully digital precoding scheme, especially for large number of data streams.

The rest of the paper is organized as follows. In Section II, the system model, channel model and the problem formulation are presented. The characteristics of spatial lobes, the equivalent spatial lobes channel and the low complexity hybrid precoding strategy are demonstrated in Section III. In Section IV, the diversity combining scheme is proposed. The simulation results are presented in Section V. Finally, we conclude this paper in Section VI.

We use the following notations in this paper:  $a$  is a scalar,  $\mathbf{a}$  is a vector,  $\mathbf{A}$  is a matrix and  $\mathcal{A}$  is a set.  $\mathbf{A}^{(i)}$  is the  $i_{th}$  column of  $\mathbf{A}$  and  $\|\mathbf{A}\|_F$  is the Frobenius norm of  $\mathbf{A}$ .  $\mathbf{A}^T, \mathbf{A}^*, \mathbf{A}^{-1}$  denote the transpose, conjugate transpose and inverse of  $\mathbf{A}$  respectively.  $\text{diag}(\mathbf{A})$  is a vector that consists of diagonal elements of  $\mathbf{A}$  and  $\text{blkdiag}(\mathbf{A}, \mathbf{B})$  is the block diagonal concatenation of  $\mathbf{A}$  and  $\mathbf{B}$ .  $[\mathbf{A} | \mathbf{B}]$  is the horizontal concatenation.  $|\mathbf{a}|$  is the modulus of  $\mathbf{a}$ .  $\mathbf{I}_N$  denotes a  $N \times N$

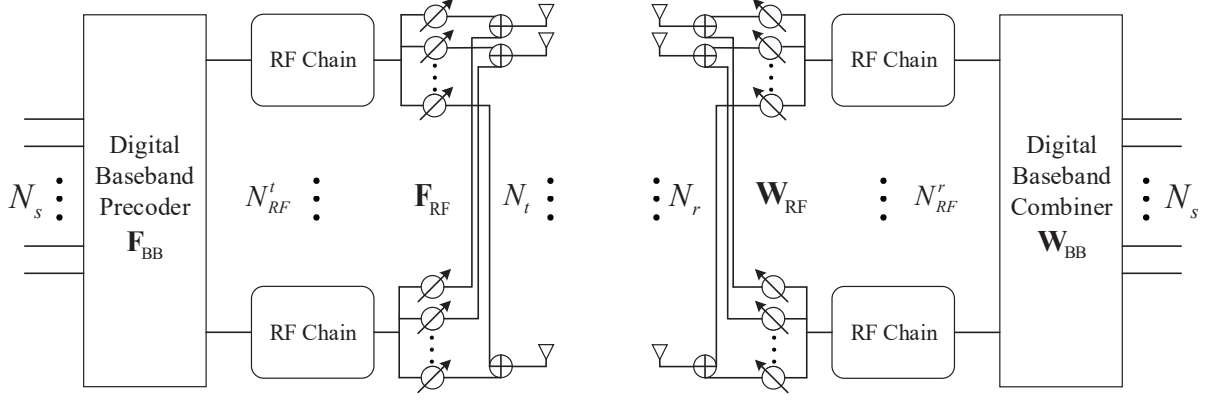


Fig. 1. Block diagram of millimeter wave MIMO system model that uses hybrid precoding structure.

identity matrix.  $\mathcal{O}(N)$  means the order is  $N$ .  $\mathcal{CN}(\mathbf{a}, \mathbf{A})$  is a complex Gaussian vector with mean  $\mathbf{a}$  and covariance matrix  $\mathbf{A}$ .  $\mathbb{E}[\mathbf{A}]$  is the expectation of  $\mathbf{A}$ .

## II. SYSTEM MODEL, CHANNEL MODEL AND PROBLEM FORMULATION

### A. System Model

We consider a single user millimeter wave MIMO system shown in Fig. 1. The transmitter and receiver are equipped with  $N_t$  and  $N_r$  antennas, respectively. The number of the RF chains at the transmitter and the receiver are respectively denoted as  $N_{\text{RF}}^t$  and  $N_{\text{RF}}^r$ , which are subject to the constraints  $N_s \leq N_{\text{RF}}^t \leq N_t$  and  $N_s \leq N_{\text{RF}}^r \leq N_r$ , where  $N_s$  denotes the number of the data streams.

At the transmitter,  $N_{\text{RF}}^t \times N_s$  baseband precoding matrix  $\mathbf{F}_{\text{BB}}$  followed by an  $N_t \times N_{\text{RF}}^t$  analog precoding matrix  $\mathbf{F}_{\text{RF}}$  transforms  $N_s$  data streams to  $N_t$  antennas. Setting  $\mathbf{F}_{\text{T}} = \mathbf{F}_{\text{RF}}\mathbf{F}_{\text{BB}}$ , the discrete-time transmitted signal vector could be written as

$$\mathbf{X} = \mathbf{F}_{\text{T}}\mathbf{s}, \quad (1)$$

where  $\mathbf{s}$  is the  $N_s \times 1$  symbol vector with  $\mathbb{E}[\mathbf{s}\mathbf{s}^*] = \frac{1}{N_s}\mathbf{I}_{N_s}$ . In this system,  $\mathbf{F}_{\text{RF}}$  is implemented by phase shifters, which has constant amplitude constraint  $(\mathbf{F}_{\text{RF}}^{(i)}\mathbf{F}_{\text{RF}}^{(i)*})_{l,l} = 1/N_t$ , where  $(\cdot)_{l,l}$  denotes the  $l_{th}$  diagonal element of a matrix. In addition, the total power constraint is enforced by  $\|\mathbf{F}_{\text{RF}}\mathbf{F}_{\text{BB}}\|_F^2 = N_s$ .

We adopt a narrowband block-fading channel model as shown in [13], [25], which yields the received signal as

$$\mathbf{r} = \sqrt{\rho}\mathbf{H}\mathbf{F}_{\text{T}}\mathbf{s} + \mathbf{n}, \quad (2)$$

where  $\mathbf{H}$  is the  $N_r \times N_t$  millimeter wave channel matrix,  $\rho$  is the average received power, and  $\mathbf{n} \sim \mathcal{CN}(0, \sigma_n^2)$  is the additive white Gaussian noise vector.

After being combined at the receiver, the received signal is

$$\mathbf{y} = \sqrt{\rho} \mathbf{W}_T^* \mathbf{H} \mathbf{F}_T \mathbf{s} + \mathbf{W}_T^* \mathbf{n}, \quad (3)$$

where  $\mathbf{W}_T = \mathbf{W}_{\text{RF}} \mathbf{W}_{\text{BB}}$ ,  $\mathbf{W}_{\text{RF}}$  is the  $N_r \times N_{\text{RF}}^r$  RF combining matrix which should satisfy  $(\mathbf{W}_{\text{RF}}^{(i)} \mathbf{W}_{\text{RF}}^{(i)*})_{l,l} = 1/N_r$  and  $\mathbf{W}_{\text{BB}}$  is the  $N_{\text{RF}}^r \times N_s$  baseband digital combining matrix.

### B. Channel Model

The millimeter wave signals have higher free-space pathloss than lower frequency signals and are very sensitive to the blockages, which lead to limited spatial scattering. Therefore, the clustered channel model is usually used to represent the millimeter wave channel [23], which could be expressed as

$$\mathbf{H} = \sqrt{\frac{N_t N_r}{MN}} \sum_{m=1}^M \sum_{n=1}^N \alpha_{m,n} \mathbf{a}_r(\theta_{m,n}^r) \mathbf{a}_t(\theta_{m,n}^t)^*, \quad (4)$$

where  $M$  is the number of clusters and each cluster contributes  $N$  propagation paths,  $\alpha_{m,n}$  denotes the complex gain of the  $n_{th}$  path in the  $m_{th}$  cluster,  $\theta_{m,n}^r \in [0, 2\pi]$  and  $\theta_{m,n}^t \in [0, 2\pi]$  are the AOA and AOD, respectively. By adopting uniform linear arrays (ULAs), the antenna array response vectors  $\mathbf{a}_r(\theta_{m,n}^r)$  and  $\mathbf{a}_t(\theta_{m,n}^t)$  at the transmitter and the receiver could be written as

$$\mathbf{a}_t(\theta_{m,n}^t) = \frac{1}{\sqrt{N_t}} \left[ 1, e^{j(2\pi/\lambda)d \sin(\theta_{m,n}^t)}, \dots, e^{j(N_t-1)(2\pi/\lambda)d \sin(\theta_{m,n}^t)} \right]^T, \quad (5)$$

and

$$\mathbf{a}_r(\theta_{m,n}^r) = \frac{1}{\sqrt{N_r}} \left[ 1, e^{j(2\pi/\lambda)d \sin(\theta_{m,n}^r)}, \dots, e^{j(N_r-1)(2\pi/\lambda)d \sin(\theta_{m,n}^r)} \right]^T, \quad (6)$$

respectively, where  $\lambda$  is the wavelength of the signal,  $d = \lambda/2$  denotes the aperture domain sample spacing. For convenient, we rewrite the channel in a more compact form as

$$\mathbf{H} = \mathbf{A}_r \text{diag}(\boldsymbol{\alpha}) \mathbf{A}_t^*, \quad (7)$$

where  $\boldsymbol{\alpha} = \sqrt{\frac{N_t N_r}{MN}} [\alpha_1, \alpha_2, \dots, \alpha_{MN}]^T$  contains the complex gains of all paths, and the matrices

$$\mathbf{A}_r = [\mathbf{a}_r(\theta_{1,1}^r), \mathbf{a}_r(\theta_{1,2}^r), \dots, \mathbf{a}_r(\theta_{1,N}^r), \dots, \mathbf{a}_r(\theta_{M,N}^r)] \quad (8)$$

and

$$\mathbf{A}_t = [\mathbf{a}_t(\theta_{1,1}^t), \mathbf{a}_t(\theta_{1,2}^t), \dots, \mathbf{a}_t(\theta_{1,N}^t), \dots, \mathbf{a}_t(\theta_{M,N}^t)] \quad (9)$$

contain the array response vectors. Inspired by (7), we could find that the number of the paths is the upper bound of the rank of the millimeter wave channel matrix.

### C. Problem Formulation

In this paper, the target of designing the hybrid precoding matrices ( $\mathbf{F}_{\text{RF}}, \mathbf{F}_{\text{BB}}, \mathbf{W}_{\text{RF}}, \mathbf{W}_{\text{BB}}$ ) is to maximize the spectral efficiency achieved with Gaussian signalling over the millimeter wave channel [26], where the spectral efficiency is given by

$$R = \log_2 \left( \left| \mathbf{I}_{N_s} + \frac{\rho}{N_s} \mathbf{R}_n^{-1} \mathbf{W}_{\text{BB}}^* \mathbf{W}_{\text{RF}}^* \mathbf{H} \mathbf{F}_{\text{RF}} \mathbf{F}_{\text{BB}} \mathbf{F}_{\text{BB}}^* \mathbf{F}_{\text{RF}}^* \mathbf{H}^* \mathbf{W}_{\text{RF}} \mathbf{W}_{\text{BB}} \right| \right), \quad (10)$$

where  $\mathbf{R}_n = \sigma_n^2 \mathbf{W}_{\text{BB}}^* \mathbf{W}_{\text{RF}}^* \mathbf{W}_{\text{RF}} \mathbf{W}_{\text{BB}}$  is the noise covariance matrix. As shown in [13], the design of precoding matrices and combining matrices could be separated. The only difference is that the combining matrices do not have an extra power constraint. Therefore, we mainly focus on the design of the precoding matrices at the transmitter and the combining matrices at the receiver could be obtained similarly. The corresponding target of designing the precoding matrices could be simplified to maximize the mutual information, which is given by

$$\mathcal{I}_t(\mathbf{F}_{\text{RF}}, \mathbf{F}_{\text{BB}}) = \log_2 \left( \left| \mathbf{I} + \frac{\rho}{N_s \sigma_n^2} \mathbf{H} \mathbf{F}_{\text{RF}} \mathbf{F}_{\text{BB}} \mathbf{F}_{\text{BB}}^* \mathbf{F}_{\text{RF}}^* \mathbf{H}^* \right| \right). \quad (11)$$

However, directly designing the precoding matrices to maximize (11) is very non-trivial. Through mathematical derivation, the hybrid precoding design problem could be formulated as an equivalent sparse reconstruction problem which is aimed to minimize the Euclidean distance between the product of the analog and digital precoding matrices and the optimal unconstrained precoding matrix [13]. The sparse reconstruction problem could be formulated as

$$\begin{aligned} (\mathbf{F}_{\text{RF}}^{\text{opt}}, \mathbf{F}_{\text{BB}}^{\text{opt}}) &= \arg \min_{\mathbf{F}_{\text{BB}}, \mathbf{F}_{\text{RF}}} \|\mathbf{F}_{\text{opt}} - \mathbf{F}_{\text{RF}} \mathbf{F}_{\text{BB}}\|_F, \\ \text{s.t. } \mathbf{F}_{\text{RF}} &\in \mathcal{F}_{\text{RF}}, \\ \|\mathbf{F}_{\text{RF}} \mathbf{F}_{\text{BB}}\|_F^2 &= N_s, \end{aligned} \quad (12)$$

where  $\mathbf{F}_{\text{opt}}$  is the optimal unconstrained precoding matrix which could be obtained from the singular value decomposition (SVD) of the millimeter wave channel  $\mathbf{H}$  and  $\mathcal{F}_{\text{RF}}$  is the set of the feasible RF precoders induced by the constant amplitude constraint. Note that, since the feasibility constraint on the RF precoding matrix is non-convex, it is very difficult to find a global optimal solution. In the design of our hybrid precoding scheme, we mainly exploit the sparseness property of the millimeter wave in the angular domain to find a low complexity near-optimal solution.

### III. PROPOSED LOW COMPLEXITY HYBRID PRECODING ALGORITHM BASED ON SPATIAL LOBES DIVISION

In this section, we firstly demonstrate the characteristic of spatial lobes of the millimeter wave channel. Then, we propose the SLD operation which reconstructs the millimeter wave channel into the equivalent spatial lobes channel. Based on the SLD operation, the low complexity hybrid precoding strategy is demonstrated in detail. We also compare the complexity of the proposed hybrid precoding scheme with the OMP scheme. Finally, we introduce several extended situations.

#### A. The Spatial Lobes Characteristics of Millimeter Wave

Recently, the millimeter wave channel was adequately measured by NYU WIRELESS which confirmed that the millimeter wave could be utilized in the 5G cellular networks [22]–[24]. The polar plot of 28 GHz millimeter wave channel for non-line-of-sight (NLOS) environment measured in Manhattan in [22] is shown in Fig. 2. At the receiver, there are five dominated spatial lobes with azimuth angle spreads, which confirms that the millimeter wave channels also have sparseness property in angular domain. In the traditional 3GPP and WINNER II channel models, which are widely used in LTE, the paths in one time cluster are assumed to arrive at a same angular spread (i.e., arrive at a same spatial lobe). Whereas the measurement results by NYU WIRELESS indicate that there are some differences between the time cluster and the spatial lobe, which are summarized as follow.

- The paths in one spatial lobe could come from more than one time cluster. Each spatial lobe represents a main AOA/AOD at which groups of multiple path components (MPCs) arrive/depart over a contiguous range of angles over several hundreds of nanoseconds. Therefore, these MPCs could come from multiple time clusters [24].
- A cluster may contain multipath components which travel close in time but arrive/depart from many angle lobe directions [23].
- The number of spatial lobes is independent of the number of time clusters [23]. Generally, the number of spatial lobes is less than that of time clusters [22], [24].

The above differences indicate that the AOAs/AODs of paths in different time clusters may be close to each other. Therefore, we could not handle different time clusters separately. In contrast, the angles of paths in different spatial lobes are sufficiently separable, which prompts

us to reconstruct the millimeter wave channel from the spatial lobes perspective and further to reduce the complexity of the hybrid precoding.

There are more descriptions about the characteristics of the spatial lobe in [22], [23]. The maximum number of the spatial lobes is 5 for the sparseness property of the millimeter wave in the angular domain. The mean angles of the spatial lobes are evenly distributed between 0 and  $2\pi$ , while the angles (AOAs/AODs) of the paths in one spatial lobe are randomly distributed within the range of the spatial lobe [22, Section II-A], [23, Section V-A].

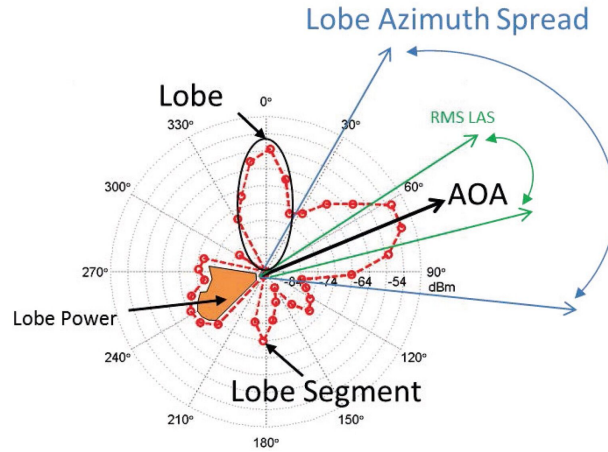


Fig. 2. The polar plot of millimeter wave channel measured in Manhattan at 28 GHz [22].

By exploiting the above characteristics of the spatial lobes and considering a relatively large number of antennas are usually employed in millimeter wave MIMO systems, we make a reasonable assumption that *the paths in different spatial lobes are orthogonal since the AOAs/AODs of these paths are sufficiently separable*. Therefore, the paths in the millimeter wave channel could be divided into several orthogonal groups according to the spatial lobe. An example of the angular domain distribution for the propagation paths considered in this paper is shown in Fig. 3, where there are four spatial lobes and each spatial lobe contains two subpaths.

### B. SLD Operation and the Equivalent Spatial Lobes Channel

As we could see, the clustered millimeter wave channel (4) is made of multiple propagation paths. Therefore, grouping the paths means dividing the channel. Based on the sparseness property of the millimeter wave in the angular domain, the SLD operation groups the total paths into several spatial lobes and reconstruct the millimeter wave channel (4) into the equivalent

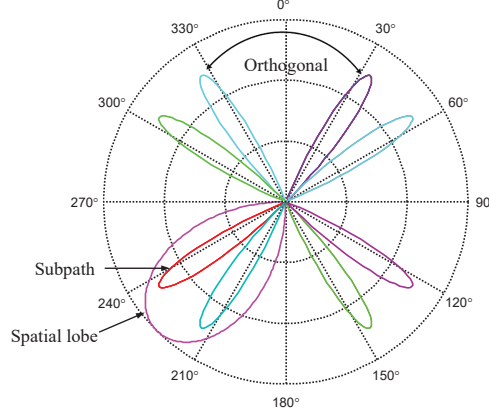


Fig. 3. An example of the angular domain paths in the millimeter wave channel, where there are four spatial lobes and each spatial lobe contains two subpaths.

spatial lobe channel. Note that, the number of groups and the number of paths in each group are the number of spatial lobes and the number of sub-paths in each spatial lobe, respectively.

We further make a reasonable assumption that *when the AODs of the paths are in one spatial lobe, the corresponding AOA will be in one spatial lobe too*. Actually, for paths in one spatial lobe at the transmitter, their AODs are close to each other. It is reasonable that the corresponding AOAs are also close to each other after passing through the wireless millimeter wave channel (reflecting, scattering and other forms of propagation). Therefore, the equivalent spatial lobes channel could be written as

$$\begin{aligned} \mathbf{H}_{sl} &= \sqrt{\frac{N_t N_r}{PQ}} \sum_{p=1}^P \sum_{q=1}^Q \alpha_{p,q} \mathbf{a}_r(\theta_{p,q}^r) \mathbf{a}_t(\theta_{p,q}^t)^* \\ &= \mathbf{H}_1 + \mathbf{H}_2 + \dots + \mathbf{H}_P, \end{aligned} \quad (13)$$

where  $\mathbf{H}_i = \sqrt{\frac{N_t N_r}{PQ}} \sum_{q=1}^Q \alpha_{i,q} \mathbf{a}_r(\theta_{i,q}^r) \mathbf{a}_t(\theta_{i,q}^t)^*$ ,  $i = 1, 2, \dots, P$  represents the  $i_{th}$  sub-channel which contains the paths in the  $i_{th}$  spatial lobe for both transmitter and receiver,  $P$  is the number of spatial lobes,  $Q$  is the number of subpaths in one spatial lobe, and  $PQ = MN$ . Note that different spatial lobes may have different number of sub-paths, we make the assumption that the numbers of sub-paths in different spatial lobes are the same to simplify the analysis. Since the paths in different spatial lobes are orthogonal, these sub-channels could be treated as orthogonal to each other. The expression form of (13) is similar as the cluster channel model (4) and could be regarded as a reconstruction of (4). Therefore, we make  $\mathbf{H} = \mathbf{H}_{sl}$  in the rest of the paper.

We could also write (13) in a more compact expression as

$$\mathbf{H} = \mathbf{A}_r \text{diag}(\boldsymbol{\alpha}) \mathbf{A}_t^*, \quad (14)$$

where  $\mathbf{A}_r = [\mathbf{a}_r(\theta_{1,1}^r), \mathbf{a}_r(\theta_{1,2}^r), \dots, \mathbf{a}_r(\theta_{1,Q}^r), \dots, \mathbf{a}_r(\theta_{P,Q}^r)]$  and  $\mathbf{A}_t = [\mathbf{a}_t(\theta_{1,1}^t), \mathbf{a}_t(\theta_{1,2}^t), \dots, \mathbf{a}_t(\theta_{1,Q}^t), \dots, \mathbf{a}_t(\theta_{P,Q}^t)]$ .

According to the spatial lobe property, the above two antenna array response matrices could be divided into several parts as

$$\mathbf{A}_t = [\mathbf{A}_{t1}, \mathbf{A}_{t2}, \dots, \mathbf{A}_{tP}], \quad (15)$$

$$\mathbf{A}_r = [\mathbf{A}_{r1}, \mathbf{A}_{r2}, \dots, \mathbf{A}_{rP}], \quad (16)$$

where

$$\mathbf{A}_{ti} = [\mathbf{a}_t(\theta_{i,1}^t), \mathbf{a}_t(\theta_{i,2}^t), \dots, \mathbf{a}_t(\theta_{i,Q}^t)], \quad i = 1, 2, \dots, P \quad (17)$$

and

$$\mathbf{A}_{ri} = [\mathbf{a}_r(\theta_{i,1}^r), \mathbf{a}_r(\theta_{i,2}^r), \dots, \mathbf{a}_r(\theta_{i,Q}^r)], \quad i = 1, 2, \dots, P \quad (18)$$

contain the antenna array response vectors of the  $i_{th}$  sub-channel. According to (14)-(18), it could be obtained that  $Q$  is the upper bound of the rank of the sub-channel. Therefore, we actually divide the millimeter wave channel into several low-rank orthogonal sub-channels.

### C. Hybrid Precoding Based on Spatial Lobes Division

In this subsection, we present a low complexity hybrid precoding scheme based on the SLD operation. In the design of the hybrid precoding, a principle of maximizing the usage of the channel is adopted, that is we keep the number of the data streams equal to the number of the total paths.

**Lemma 1:** (from [27]). *Each left and right singular vectors corresponding to non-zero eigenvalues of the matrix channel converge in chordal distance to the array response vectors when the number of the total paths ( $L$ ) in the channel is much less than the number of antennas at both transmitter and receiver, i.e.,  $L = o(N_t)$  and  $L = o(N_r)$ .*

Lemma 1 demonstrates that the array response vectors are approximate orthogonal with each other and the channel representation (14) “converges” to the SVD of  $\mathbf{H}$  for large number of the antennas.

**Corollary 1:** *When  $L \ll \min(N_t, N_r)$ , the left and right singular matrices of the total channel matrix  $\mathbf{H}$  consist of the left and right singular vectors from the sub-channels, respectively.*

*Proof 1:* For the  $i_{th}$  sub-channel, we have

$$\mathbf{H}_i = \mathbf{A}_{ri} \text{diag}(\boldsymbol{\alpha}_i) \mathbf{A}_{ti}^* = \mathbf{U}_i \boldsymbol{\Sigma}_i \mathbf{V}_i^*. \quad (19)$$

According to (15) and (16), the total array response matrices consist of the array response matrices for each sub-channel. In the meantime, according to Lemma 1, we could conclude that left and right singular vectors corresponding to the  $Q$  largest singular values in  $\mathbf{U}_i$  and  $\mathbf{V}_i^*$  converge in chordal distance to the responding array response vectors in  $\mathbf{A}_{ri}$  and  $\mathbf{A}_{ti}$ , respectively.

Since the left and right singular matrices are the optimal unconstrained fully digital precoding matrices, Corollary 1 indicates that, the design of the precoding matrix for the total channel matrix could be divided into the precoding design for each sub-channel when  $L \ll \min(N_t, N_r)$ . Note that the angles of antenna response vectors for different spatial lobes are sufficiently separable, which makes the “inter-lobes” interference very small. Thus, even the antenna response vectors are not orthogonal to each other for the antennas array of practical size (required by millimeter wave wave communications), we could still divide the total hybrid precoding problem into several subproblems, each of which is only designed for one sub-channel.

Therefore, for the  $i_{th}$  spatial lobe or sub-channel, the optimization problem could be formulated as

$$\begin{aligned} (\mathbf{F}_{RF_i}^{\text{opt}}, \mathbf{F}_{BB_i}^{\text{opt}}) &= \arg \min_{\mathbf{F}_{BB_i}, \mathbf{F}_{RF_i}} \|\mathbf{F}_{\text{opt}_i} - \mathbf{F}_{RF_i} \mathbf{F}_{BB_i}\|_F, \\ \text{s.t. } \mathbf{F}_{RF_i} &\in \mathcal{F}_{RF}, \\ \|\mathbf{F}_{RF_i} \mathbf{F}_{BB_i}\|_F^2 &= N_s \frac{A_i}{\sum_{i=1}^P A_i}, \end{aligned} \quad (20)$$

where  $\mathbf{F}_{\text{opt}_i} = \mathbf{V}_i(:, 1 : Q)$  is the optimal reference precoding matrix,  $\mathbf{F}_{RF_i}$  and  $\mathbf{F}_{BB_i}$  are the analog precoding matrix and digital precoding matrix for the  $i_{th}$  sub-channel, respectively.  $\mathcal{F}_{RF} = \bigcup_{i=1,2,\dots,P} \mathcal{F}_{RF_i}$  is the set of the feasible RF precoders and  $\mathcal{F}_{RF_i}$  is the feasible set of RF precoder for the  $i_{th}$  sub-channel.  $A_i$  is the total power in the  $i_{th}$  spatial lobe and we assume equal power distribution in this paper.

Note that, since the number of paths  $Q$  in each sub-channel is very small, i.e.,  $Q \ll \min(N_t, N_r)$ , the sub-channel could be considered to be in a very poor scattering environment. Inspired by Lemma 1, in the proposed hybrid precoding scheme, we set the antenna array response matrices  $\mathbf{A}_{ti}$  and  $\mathbf{A}_{ri}$  as the reference matrices  $\mathbf{F}_{\text{res}}$ , rather than the fully digital precoding matrix obtained by high-dimensional SVD, for the  $i_{th}$  sub-channel. However, for arrays of practical sizes, only setting  $\mathbf{A}_{ti}$  and  $\mathbf{A}_{ri}$  as the reference precoding matrices may cause many performance losses.

Therefore, we further perform a digital precoding design at the baseband. In summary, in our hybrid precoding scheme, we decouple the solution of the optimization problem (20) into analog and digital phases, where the target of the analog precoding is to find the constant amplitude vectors which are closest to each entry of the  $\mathbf{F}_{\text{res}}$  in the  $l_2$  norm sense, and the digital precoding is aimed to remove the interference and perform power allocation to these vectors. We demonstrate the design of the analog and digital precoding matrices in detail as follows.

**Lemma 2:** *For the selected vectors of different sub-channels, there is no overlap between the corresponding feasible sets  $\mathcal{F}_{\text{RF}_i}, i = 1, 2, \dots, P$ .*

*Proof 2:* Define the beam width of the  $i_{th}$  spatial lobe as

$$\mathcal{CV}(SL_i) = \bigcup_{j=1,2,\dots,Q} \mathcal{CV}(a(\theta_{i,j}^t)), \quad i = 1, 2, \dots, P, \quad (21)$$

where  $\mathcal{CV}(a(\theta_{i,j}^t))$  is the beam width of the steering vectors in the  $i_{th}$  spatial lobe (sub-channel). For the ULA considered in this paper, the half-power beam width of the array is approximately equal to  $102^\circ/N$  [28], where  $N$  is the number of antennas, i.e.,  $\mathcal{CV}(a(\theta_{i,j}^t)) = 102^\circ/N$ . Therefore, we have

$$\frac{102^\circ}{N} \leq \mathcal{CV}(SL_i) \leq Q \frac{102^\circ}{N}. \quad (22)$$

As shown in Fig. 3, the AOAs and AODs in different spatial lobes are sufficiently separable. When the angle interval  $\Delta_\theta$  between the mean angles of different spatial lobes satisfies

$$\Delta_\theta > Q \frac{102^\circ}{N}, \quad (23)$$

there will be no overlap between different spatial lobes. Moreover, since the angles of  $\mathcal{CV}(\mathcal{F}_{\text{RF}_i})$  could not exceed the range of the  $i_{th}$  spatial lobe, we have

$$\mathcal{CV}(\mathcal{F}_{\text{RF}_i}) \subseteq \mathcal{CV}(SL_i). \quad (24)$$

Therefore, there will be no overlap between the different feasible sets.

Lemma 2 indicates that the selected vectors for different sub-channel cause small interference with each other and the total feasible set  $\mathcal{F}_{\text{RF}}$  could be simply divided into  $P$  parts for each sub-channel to select the vectors in parallel. Actually, this is why we assume that the paths in

different spatial lobes are orthogonal with each other in section III.A. Therefore, (20) could be simplified as

$$\begin{aligned}
(\mathbf{F}_{\text{RF}_i}^{\text{opt}}, \mathbf{F}_{\text{BB}_i}^{\text{opt}}) &= \arg \min_{\mathbf{F}_{\text{BB}_i}, \mathbf{F}_{\text{RF}_i}} \|\mathbf{F}_{\text{opt}_i} - \mathbf{F}_{\text{RF}_i} \mathbf{F}_{\text{BB}_i}\|_F, \\
\text{s.t. } \mathbf{F}_{\text{RF}_i} &\in \mathcal{F}_{\text{RF}_i}, \\
\|\mathbf{F}_{\text{RF}_i} \mathbf{F}_{\text{BB}_i}\|_F^2 &= N_s \frac{A_i}{\sum_{i=1}^P A_i},
\end{aligned} \tag{25}$$

In the analog precoding phase, to make the precoding scheme more practical for the limited feedback system, the feasible sets are quantized with limited  $b$  bits [29]. The quantized candidate matrix for the transmitter is

$$\mathbf{A}_t^{\text{quant}} = [a_t^{\text{quant}}(\theta_1), a_t^{\text{quant}}(\theta_2), \dots, a_t^{\text{quant}}(\theta_{2^b})], \tag{26}$$

where the entries of  $\mathbf{A}_t^{\text{quant}}$  are

$$a_t^{\text{quant}}(\theta_i) = \frac{1}{\sqrt{N_t}} \left[ 1, e^{j\pi \sin(\frac{2\pi(i-1)}{2^b})}, \dots, e^{j(N_t-1)\pi \sin(\frac{2\pi(i-1)}{2^b})} \right]^T. \tag{27}$$

Note that, the quantization candidate matrix divides the angular domain space into  $2^b$  parts uniformly, and could be further divided into  $P$  spatial lobes parts as

$$\mathbf{A}_t^{\text{quant}} = [\mathbf{A}_{t1}^{\text{quant}}, \mathbf{A}_{t2}^{\text{quant}}, \dots, \mathbf{A}_{tP}^{\text{quant}}]. \tag{28}$$

The selection of quantization bit is related to the number of antennas. Generally, we should at least make the quantization bit satisfy  $2^b \geq \max(N_t, N_r)$  to guarantee good performance. However, the complexity increases exponentially with the quantization bit. Therefore, selecting a reasonable quantization bit is important, and the corresponding simulation will be presented in Section V.

Given the quantization matrices, the remaining operations in the analog precoding phase are to find the vectors form the quantization matrices which are closest to each entry of the  $\mathbf{F}_{\text{res}}$  in the  $l_2$  norm sense. This is equivalent to find the vectors along which the reference matrix  $\mathbf{F}_{\text{res}}$  has the maximum projection. We only introduce the analog precoding design at the transmitter, while the the analog precoding matrix at the receiver could be obtained in the same way. The correlation matrix is

$$\mathbf{\Psi} = \mathbf{A}_{ti}^{\text{quant}*} \mathbf{F}_{\text{res}}. \tag{29}$$

The power distributed in each direction could be calculated as

$$\mathbf{k} = \text{diag}(\mathbf{\Psi} \mathbf{\Psi}^*). \tag{30}$$

Then, we select the position indexes of the  $Q$  largest values in  $\mathbf{k}$ , and obtain the corresponding vectors from the quantization matrices. Once a vector has been selected, the value of the corresponding location in  $\mathbf{k}$  is set to be zero to eliminate the effects of the vector. According to (29) and (30), the analog precoding matrix for the  $i_{th}$  sub-channel could be obtained as

$$\mathbf{F}_{\text{RF}_i} = [\mathbf{F}_{\text{RF}_{i1}}, \mathbf{F}_{\text{RF}_{i2}}, \dots, \mathbf{F}_{\text{RF}_{iQ}}], i = 1, 2, \dots, P, \quad (31)$$

where  $\mathbf{F}_{\text{RF}_{ij}}$  represents the selected vectors steering at the  $j_{th}$  paths in the  $i_{th}$  sub-channel. After the analog precoding matrices for all sub-channels are obtained, the final analog precoding matrix at the transmitter could be determined by

$$\mathbf{F}_{\text{RF}} = [\mathbf{F}_{\text{RF}_1}, \mathbf{F}_{\text{RF}_2}, \dots, \mathbf{F}_{\text{RF}_P}]. \quad (32)$$

Note that, since the selected vectors  $\mathbf{F}_{\text{RF}_{ij}}$  are not orthogonalized, we only need to find these vectors to steer at the paths and leave the orthogonalization process to the digital precoding phase. In the similar way, the analog precoding matrix at the receiver could be obtained as

$$\mathbf{W}_{\text{RF}} = [\mathbf{W}_{\text{RF}_1}, \mathbf{W}_{\text{RF}_2}, \dots, \mathbf{W}_{\text{RF}_P}]. \quad (33)$$

If the exact AOAs and AODs that make up the array response vectors are not known in advance, we could also utilize corresponding channel estimation scheme to obtain the estimated AOAs and AODs, e.g., the adaptive estimation algorithm for multi-path mmWave channel proposed in [25]. In the meantime, considering the spatial lobes characteristic of the millimeter wave channel, the complexity of the channel estimation algorithm could also be reduced by dividing the total channel into several sub-channels. In practice, after the channel estimation, the angles of paths could be obtained. Then, we could group the paths whose angles are relatively close, which is the SLD operation introduced in Section III-B. The number of groups is the number of spatial lobes and the number of the paths in each group is the corresponding number of sub-paths in each spatial lobe.

*Remark 1:* In the analog precoding phase, only  $Q$  RF chains are actually utilized for each spatial lobe. Therefore, we only utilize total  $PQ$  RF chains at both the transmitter and receiver, which will save the power consumption. Moreover, when the number of the RF chains satisfy  $N_{\text{RF}}^{\text{r}} \geq PQ$  and  $N_{\text{RF}}^{\text{t}} \geq PQ$ , the analog precoding matrices of these  $P$  sub-channels could be obtained in parallel.

After the analog precoding phase, we obtain the effective low-dimensional channel as

$$\begin{aligned}
\mathbf{H}_{\text{eq}} &= \mathbf{W}_{\text{RF}}^* \mathbf{H} \mathbf{F}_{\text{RF}} \\
&= [\mathbf{W}_{\text{RF}_1}, \mathbf{W}_{\text{RF}_2}, \dots, \mathbf{W}_{\text{RF}_P}]^* \mathbf{H} [\mathbf{F}_{\text{RF}_1}, \mathbf{F}_{\text{RF}_2}, \dots, \mathbf{F}_{\text{RF}_P}] \\
&= \begin{bmatrix} \mathbf{W}_{\text{RF}_1}^* \mathbf{H} \mathbf{F}_{\text{RF}_1}, & \mathbf{W}_{\text{RF}_1}^* \mathbf{H} \mathbf{F}_{\text{RF}_2}, & \dots, & \mathbf{W}_{\text{RF}_1}^* \mathbf{H} \mathbf{F}_{\text{RF}_P} \\ \mathbf{W}_{\text{RF}_2}^* \mathbf{H} \mathbf{F}_{\text{RF}_1}, & \mathbf{W}_{\text{RF}_2}^* \mathbf{H} \mathbf{F}_{\text{RF}_2}, & \dots, & \mathbf{W}_{\text{RF}_2}^* \mathbf{H} \mathbf{F}_{\text{RF}_P} \\ \vdots & \vdots & \ddots & \vdots \\ \mathbf{W}_{\text{RF}_P}^* \mathbf{H} \mathbf{F}_{\text{RF}_1}, & \mathbf{W}_{\text{RF}_P}^* \mathbf{H} \mathbf{F}_{\text{RF}_2}, & \dots, & \mathbf{W}_{\text{RF}_P}^* \mathbf{H} \mathbf{F}_{\text{RF}_P} \end{bmatrix} \\
&= \begin{bmatrix} \tilde{\mathbf{H}}_{11}, \tilde{\mathbf{H}}_{12}, \dots, \tilde{\mathbf{H}}_{1P} \\ \tilde{\mathbf{H}}_{21}, \tilde{\mathbf{H}}_{22}, \dots, \tilde{\mathbf{H}}_{2P} \\ \vdots & \vdots & \ddots & \vdots \\ \tilde{\mathbf{H}}_{P1}, \tilde{\mathbf{H}}_{P2}, \dots, \tilde{\mathbf{H}}_{PP} \end{bmatrix}, \tag{34}
\end{aligned}$$

where  $\mathbf{H}_{\text{eq}}$  is a  $PQ \times PQ$  matrix and  $\tilde{\mathbf{H}}_{ij} \in \mathbb{C}^{Q \times Q}$  are called as effective sub-channels. According to (14), we could find that  $\mathbf{W}_{\text{RF}_i}$  and  $\mathbf{F}_{\text{RF}_i}$  are one by one correspondence for the  $i_{th}$  sub-channel. Therefore, only the diagonal effective sub-channels make sense, and (34) could be rewritten as

$$\tilde{\mathbf{H}}_{\text{eq}} = \begin{bmatrix} \tilde{\mathbf{H}}_{11} & & & \\ & \tilde{\mathbf{H}}_{22} & & \\ & & \ddots & \\ & & & \tilde{\mathbf{H}}_{PP} \end{bmatrix}, \tag{35}$$

where  $\tilde{\mathbf{H}}_{ii}$  contains the paths whose AODs and AOAs respectively belong to the  $i_{th}$  spatial lobe at the transmitter and the receiver.

**Lemma 3:** The left and right singular matrices of the effective channel  $\tilde{\mathbf{H}}_{\text{eq}}$  could be directly obtained by applying SVD for each effective sub-channel  $\tilde{\mathbf{H}}_{ii}, i = 1, 2, \dots, P$ .

*Proof 3:* For each effective sub-channel, we have

$$\tilde{\mathbf{H}}_{ii} = \tilde{\mathbf{U}}_{ii} \tilde{\Sigma}_{ii} \tilde{\mathbf{V}}_{ii}^*, i = 1, 2, \dots, P, \tag{36}$$

where  $\tilde{\mathbf{U}}_{ii}$  and  $\tilde{\mathbf{V}}_{ii}$  are the left and right singular matrices of  $\mathbf{H}_{ii}$  and  $\Sigma_{ii}$  is a diagonal matrix with the singular values arranged in decreasing order. Therefore, the effective channel (35) could

---

**Algorithm 1** Hybrid Precoding Based on Spatial Lobes Division (HYP-SLD)
 

---

**Input:**  $\mathbf{A}_t, \mathbf{A}_r, \mathbf{A}_t^{\text{quant}}, \mathbf{A}_r^{\text{quant}}$ 
**Output:**  $\mathbf{F}_{\text{RF}}, \mathbf{F}_{\text{BB}}, \mathbf{W}_{\text{RF}}, \mathbf{W}_{\text{BB}}$ 

```

1: for  $i \leq P$  do
2:    $\mathbf{F}_{\text{res}} = \mathbf{A}_{ti}$ 
3:    $\Psi = \mathbf{A}_{ti}^{\text{quant}*} \mathbf{F}_{\text{res}}$ 
4:   for  $j \leq Q$  do
5:      $k = \text{argmax}_{l=1,\dots,Q} \text{diag}(\Psi \Psi^*)$ 
6:      $\mathbf{F}_{\text{RF}_i} = \left[ \mathbf{F}_{\text{RF}_i} \mid \mathbf{A}_{ti}^{\text{quant}(k)} \right]$ 
7:      $\text{diag}(\Psi \Psi^*)(l) = 0$ 
8:   end for
9: end for
10:  $\mathbf{F}_{\text{RF}} = [\mathbf{F}_{\text{RF}_1}, \mathbf{F}_{\text{RF}_2}, \dots, \mathbf{F}_{\text{RF}_P}]$ 
11: We could obtain  $\mathbf{W}_{\text{RF}}$  in the same way
12:  $\mathbf{W}_{\text{RF}} = [\mathbf{W}_{\text{RF}_1}, \mathbf{W}_{\text{RF}_2}, \dots, \mathbf{W}_{\text{RF}_P}]$ 
13:  $\mathbf{H}_{\text{eq}} = \mathbf{W}_{\text{RF}}^* \mathbf{H} \mathbf{F}_{\text{RF}}$ 
14: for  $i \leq P$  do
15:   Compute the SVD of  $\mathbf{W}_{\text{RF}_i}^* \mathbf{H} \mathbf{F}_{\text{RF}_i}$  from  $\mathbf{H}_{\text{eq}}$ 
16:    $\mathbf{W}_{\text{RF}_i}^* \mathbf{H} \mathbf{F}_{\text{RF}_i} = \mathbf{U}_{ii} \Sigma_{ii} \mathbf{V}_{ii}^*$ 
17:    $\mathbf{F}_{\text{BB}_i} = \mathbf{V}_{ii}, \mathbf{W}_{\text{BB}_i} = \mathbf{U}_{ii}$ 
18: end for
19:  $\mathbf{F}_{\text{BB}} = \text{blkdiag}(\mathbf{F}_{\text{BB}_1}, \mathbf{F}_{\text{BB}_2}, \dots, \mathbf{F}_{\text{BB}_P})$ 
20:  $\mathbf{W}_{\text{BB}} = \text{blkdiag}(\mathbf{W}_{\text{BB}_1}, \mathbf{W}_{\text{BB}_2}, \dots, \mathbf{W}_{\text{BB}_P})$ 
21:  $\mathbf{F}_{\text{BB}} = \sqrt{N_s \frac{\mathbf{F}_{\text{BB}}}{\|\mathbf{F}_{\text{RF}} \mathbf{F}_{\text{BB}}\|_F}}$ 

```

---

be written as

$$\begin{aligned}
 \tilde{\mathbf{H}}_{\text{eq}} &= \begin{bmatrix} \tilde{\mathbf{U}}_{11} \tilde{\Sigma}_{11} \tilde{\mathbf{V}}_{11}^* & & & \\ & \tilde{\mathbf{U}}_{22} \tilde{\Sigma}_{22} \tilde{\mathbf{V}}_{22}^* & & \\ & & \ddots & \\ & & & \tilde{\mathbf{U}}_{PP} \tilde{\Sigma}_{PP} \tilde{\mathbf{V}}_{PP}^* \end{bmatrix} \\
 &= \tilde{\mathbf{U}} \tilde{\Sigma} \tilde{\mathbf{V}}^*,
 \end{aligned} \tag{37}$$

where

$$\tilde{\mathbf{U}} = \begin{bmatrix} \tilde{\mathbf{U}}_{11} & & & \\ & \tilde{\mathbf{U}}_{22} & & \\ & & \ddots & \\ & & & \tilde{\mathbf{U}}_{PP} \end{bmatrix}, \quad (38)$$

$$\tilde{\mathbf{\Sigma}} = \begin{bmatrix} \tilde{\Sigma}_{11} & & & \\ & \tilde{\Sigma}_{22} & & \\ & & \ddots & \\ & & & \tilde{\Sigma}_{PP} \end{bmatrix}, \quad (39)$$

$$\tilde{\mathbf{V}} = \begin{bmatrix} \tilde{\mathbf{V}}_{11} & & & \\ & \tilde{\mathbf{V}}_{22} & & \\ & & \ddots & \\ & & & \tilde{\mathbf{V}}_{PP} \end{bmatrix}. \quad (40)$$

Since  $\tilde{\mathbf{U}}_{ii}$  and  $\tilde{\mathbf{V}}_{ii}$  are unitary matrices and  $\tilde{\Sigma}_{ii}$  is a diagonal matrix of non-negative elements,  $\tilde{\mathbf{U}}\tilde{\mathbf{\Sigma}}\tilde{\mathbf{V}}^*$  is a singular value decomposition of the channel  $\tilde{\mathbf{H}}_{\text{eq}}$ .

Note that, since there is no constant magnitude constrains in the digital precoding phase, the digital precoding matrices could be directly obtained by applying SVD. According to Lemma 3, the digital precoding matrices for the transmitter and receiver could be easily determined as

$$\mathbf{F}_{\text{BB}} = \tilde{\mathbf{V}}, \quad (41)$$

$$\mathbf{W}_{\text{BB}} = \tilde{\mathbf{U}}. \quad (42)$$

Finally, the precoding matrices are normalized to satisfy the power constrains at the transmitter. The proposed scheme is described in detail in **Algorithm 1**.

#### D. Computational Complexity Analysis

In this subsection, we briefly analyze the complexity of proposed HYP-SLD hybrid precoding scheme. Compared with the OMP scheme, the reduction in complexity is mainly reflected in the following aspects.

1) *The optimal fully digital precoding is not needed in advance.* Considering that the optimal precoding matrices converge in chordal distance to antennal response matrices for limited scattering paths [27], we set  $\mathbf{A}_{\text{ti}}$  and  $\mathbf{A}_{\text{ri}}$  rather than the fully digital precoding matrices as the

TABLE I  
THE COMPUTATIONAL COMPLEXITY FOR DIFFERENT HYBRID PRECODING SCHEMES AT THE  
TRANSMITTER

Computation \ Scheme	OMP	HYP-SLD
$\mathbf{F}_{\text{opt}}$	$\mathcal{O}(N_t^2 N_r + N_r^3)$	NULL
Analog precoding matrix	$\mathcal{O}(2^b N_t N_{\text{RF}}^t N_s)$	$\mathcal{O}(2^b N_t Q)$
Digital precoding matrix	$\mathcal{O}((N_{\text{RF}}^t)^2 N_t (N_{\text{RF}}^t + N_s))$	$\mathcal{O}(PQ^3)$

reference matrices for the  $i_{th}$  sub-channel, which could avoid SVD operation of high-dimensional channel matrix.

2) *The search space of the selected analog precoding vectors is reduced.* In the analog precoding phase, both the candidate matrix and the reference matrix are divided into  $P$  parts according to the spatial lobes. For the  $i_{th}$  sub-channel, we only need to select the vector from the corresponding part of the quantization matrix, along which the corresponding part of the reference matrix has the maximum projection. The above operations are shown from step 2 to step 8 in **Algorithm 1**.

3) *The SVD in digital precoding phase is divided.* After the analog precoding phase, we obtain the digital domain millimeter wave channel  $\mathbf{H}_{\text{eq}}$  with  $PQ \times PQ$  dimension. Since the effective sub-channels make up a block diagonal matrix  $\tilde{\mathbf{H}}_{\text{eq}}$ , we are able to handle each effective sub-channel separately to obtain the digital precoding matrices, which is actually implemented by performing SVD shown as (37).

The computation complexities for all hybrid precoding design phases at the transmitter are summarized in Table I. The complexity of computing precoding matrices at both the transmitter and the receiver doubles the number of the operations, while the order of the overall complexity unchanged. Taking  $N_t = 64$ ,  $N_r = 32$ ,  $N_{\text{RF}}^t = 16$ ,  $N_{\text{RF}}^r = 8$ ,  $P = 4$ ,  $Q = 2$ ,  $b = 7$ ,  $N_s = PQ = N_{\text{RF}}^r$  for example, we find that the reduction of the complexity is more than 99% compared with the OMP scheme.

### E. Extended Situations

1) *The Multi-User MIMO System.* Though the proposed hybrid precoding scheme in this paper is designed for single-user MIMO system, it could be easily extended to multi-user multiple-input multiple-output (MU-MIMO) system and could reduce the computation complexity dramatically. For downlink transmission, when users are sufficiently separable, they could be distinguished and signals are transmitted through spatial division multiple access (SDMA) [30]. However, for the users whose locations are close to each other, the interference between them will be very large. Fortunately, considering the characteristic of the spatial lobes in the angular domain, we could intuitively allocate different SLs to the users to transmit signals with negligible interference.

2) *The Partially Connected Structure.* In this structure, each RF chain is only connected with partially antennas which form a sub-array. We could directly choose each RF chain to control each sub-array separately to transmit signals along each spatial lobe. This partially connected structure has lower hardware complexity with some performance losses. Therefore, it is more suitable for the energy efficient systems.

3) *Other Type of Antenna Arrays.* For uniform planar array (UPA) and uniform circular array (UCA), the angular domain is extended to two-dimensional space. Accompanied by the expansion of space is the great increases in complexity to select the vectors in the analog precoding phase. Therefore, reducing the complexity of hybrid precoding strategy is significant. Fortunately, the azimuth angles still have sparse property and could also be divided into several spatial lobes. As for the elevation angles, they always have smaller angle spread.

## IV. PROPOSED SPATIAL LOBES DIVERSITY COMBINING SCHEME HYP-SLD-MRC

In the HYP-SLD hybrid precoding scheme, the singular values matrix of  $\tilde{\mathbf{H}}_{\text{eq}}$  is

$$\tilde{\Sigma} = \begin{bmatrix} \tilde{\Sigma}_{11} & & & \\ & \tilde{\Sigma}_{22} & & \\ & & \ddots & \\ & & & \tilde{\Sigma}_{PP} \end{bmatrix}, \quad (43)$$

where

$$\tilde{\Sigma}_{ii} = \begin{bmatrix} \tilde{\Sigma}_{ii1} & & & \\ & \tilde{\Sigma}_{ii2} & & \\ & & \ddots & \\ & & & \tilde{\Sigma}_{iiQ} \end{bmatrix}, i = 1, 2, \dots, P, \quad (44)$$

contains the singular values for the  $i_{th}$  spatial lobe and  $\tilde{\Sigma}_{ii1} \geq \tilde{\Sigma}_{ii2} \geq \dots \geq \tilde{\Sigma}_{iiQ}$ . Moreover, it could be observed that  $\tilde{\Sigma}_{ii}$  has at least one dominated singular value of the total channel matrix  $\mathbf{H}$  when the AOAs and AODs of different spatial lobes are sufficiently separable. We find that the data streams are associated with the subpaths in each spatial lobe, which inspires us to further utilize these subpaths. Since the number of data streams is equal to the number of paths, all singular values including the relatively small singular values are used to transmit signals, which causes poor BER performance. Therefore, we design a simple diversity combining scheme to improve the BER performance in the rest of this section. Specifically, we firstly introduce the classic maximal-ratio combining (MRC) diversity combining technique [31]. Then, we propose a new type of diversity combining scheme based on MRC.

#### A. Maximal-Ratio Combining Scheme

In a SIMO system where the receiver is equipped with  $N$  antennas, the received signal vector is

$$\mathbf{y}_{\text{mrc}} = \mathbf{h}s_{\text{mrc}} + \mathbf{n}, \quad (45)$$

where  $\mathbf{h} = [h_0, h_1, \dots, h_{N-1}]^T$  represents the channel gain vector,  $s_{\text{mrc}}$  is the unit power signal transmitted and  $\mathbf{n}$  is additive white gaussian noise. MRC conducts a weighted sum across all branches (antennas) with the objective of maximizing SNR [31], where the weight vector is

$$\mathbf{w}_{\text{mrc}} = \frac{\mathbf{h}^*}{\|\mathbf{h}\|}. \quad (46)$$

The output signal could be obtained by

$$\hat{\mathbf{y}}_{\text{mrc}} = \mathbf{w}_{\text{mrc}}\mathbf{y}_{\text{mrc}}. \quad (47)$$

Since the signal  $s_{\text{mrc}}$  has unit average power, the instantaneous output SNR could be calculated by

$$\begin{aligned} \gamma &= \frac{|\mathbf{h}^*\mathbf{h}|^2}{\sigma^2\mathbf{h}^*\mathbf{h}} = \frac{\mathbf{h}^*\mathbf{h}}{\sigma^2} = \sum_{n=0}^{N-1} \frac{|h_n|^2}{\sigma^2} \\ &= \sum_{n=0}^{N-1} \gamma_n, \end{aligned} \quad (48)$$

where  $\gamma_n$  is the input SNR at the  $n_{th}$  antenna. As we can see, the output SNR is the summation of the input SNRs, which is actually the maximum output SNR. Therefore, the output signal achieves better BER performance due to the increase of the SNR. Generally, the variable gain weighting factor  $\mathbf{w}_{\text{mrc}}$  could be set to be the ratio of the signal amplitude to the noise power for the diversity path, which has been proved in [31].

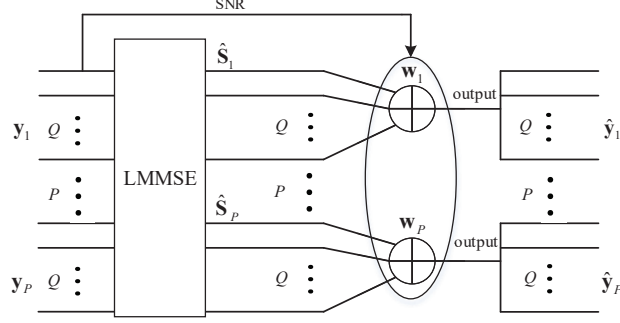


Fig. 4. The block diagram of the proposed HYP-SLD-MRC diversity combining scheme.

### B. Proposed HYP-SLD-MRC Diversity Combining Scheme

In this subsection, we demonstrate the proposed HYP-SLD-MRC diversity combining scheme which is shown in Fig. 4. According to the singular values matrix (47), we find that each sub-channel contains at least a dominated singular value of the total channel. Meanwhile, since the number of subpaths satisfies  $Q \ll \min(N_t, N_r)$ , there is no strong correlation between the data streams on different subpaths. Therefore, we could perform the diversity combining scheme in each sub-channel.

At the transmitter, the signals in (1) are divided into  $P$  blocks, which is given by

$$\mathbf{s} = [\mathbf{s}_1, \mathbf{s}_2, \dots, \mathbf{s}_P]^T, \quad (49)$$

where  $\mathbf{s}_i$ ,  $i = 1, 2, \dots, P$ , contains  $Q$  copies of one signal transmitted along the  $i_{th}$  spatial lobe (sub-channel), i.e.,

$$\mathbf{s}_i = [s_{i1}, s_{i2}, \dots, s_{iQ}]^T, \quad (50)$$

and

$$s_{i1} = s_{i2} = \dots = s_{iQ}. \quad (51)$$

The above signals are transmitted using the millimeter wave channel based on the proposed HYP-SLD precoding scheme. Therefore, we associate  $\mathbf{s}_i$  with the  $i_{th}$  sub-channel. At the receiver,

linear minimum mean square error (LMMSE) demodulator is utilized to demodulate the received signal  $\mathbf{y}$  in (3). The demodulated signal vector could be obtained by

$$\begin{aligned}
\hat{\mathbf{s}} &= (\hat{\mathbf{H}}^* \hat{\mathbf{H}} + \sigma^2 \mathbf{I})^{-1} \hat{\mathbf{H}}^* \mathbf{y} \\
&= (\hat{\mathbf{H}}^* \hat{\mathbf{H}} + \sigma^2 \mathbf{I})^{-1} \hat{\mathbf{H}}^* \hat{\mathbf{H}} \mathbf{s} + (\hat{\mathbf{H}}^* \hat{\mathbf{H}} + \sigma^2 \mathbf{I})^{-1} \hat{\mathbf{H}}^* \mathbf{W}_T^* \mathbf{n} \\
&= [\hat{\mathbf{s}}_1, \hat{\mathbf{s}}_2, \dots, \hat{\mathbf{s}}_P]^T \\
&= [\hat{s}_{11}, \hat{s}_{12}, \dots, \hat{s}_{1Q}, \dots, \hat{s}_{PQ}]^T,
\end{aligned} \tag{52}$$

where  $\hat{\mathbf{H}} = \mathbf{W}_{\text{BB}}^* \mathbf{W}_{\text{RF}}^* \mathbf{H} \mathbf{F}_{\text{RF}} \mathbf{F}_{\text{BB}}$ , and  $\hat{\mathbf{s}}_i$  contains  $Q$  received copies transmitted along the  $i_{th}$  sub-channel.

To maximize the output SNR for each sub-channel, we adopt the concept of MRC to combine the  $Q$  signal copies of  $\hat{\mathbf{s}}_i, i = 1, 2, \dots, P$ . Since the power of the transmitted symbol is normalized, the received signal amplitude after demodulation could be written as

$$P_s = \frac{\|\hat{\mathbf{H}}\|_F^2}{\|\hat{\mathbf{H}}^* \hat{\mathbf{H}} + \sigma^2 \mathbf{I}\|_F}. \tag{53}$$

The noise power is

$$\begin{aligned}
P_n &= (\hat{\mathbf{H}}^* \hat{\mathbf{H}} + \sigma^2 \mathbf{I})^{-1} \hat{\mathbf{H}}^* \mathbf{W}_T^* \mathbf{n} * ((\hat{\mathbf{H}}^* \hat{\mathbf{H}} + \sigma^2 \mathbf{I})^{-1} \hat{\mathbf{H}}^* \mathbf{W}_T^* \mathbf{n})^* \\
&= \frac{\sigma^2 \|\hat{\mathbf{H}}^* \mathbf{W}_T^*\|_F^2}{\|\hat{\mathbf{H}}^* \hat{\mathbf{H}} + \sigma^2 \mathbf{I}\|_F^2}.
\end{aligned} \tag{54}$$

Since the analog precoding matrices are selected from the quantized candidate matrices and the digital precoding matrices are unitary matrices, we have

$$\mathbf{W}_T^* \mathbf{W}_T = \mathbf{I}_{N_s}. \tag{55}$$

Therefore, (56) could be simplified as

$$P_n = \frac{\sigma^2 \|\hat{\mathbf{H}}^*\|_F^2}{\|\hat{\mathbf{H}}^* \hat{\mathbf{H}} + \sigma^2 \mathbf{I}\|_F^2}. \tag{56}$$

Then, the weight value for the total signals could be computed by

$$\begin{aligned}
\hat{w} &= \frac{P_s}{P_n} \\
&= \frac{\|\hat{\mathbf{H}}^* \hat{\mathbf{H}} + \sigma^2 \mathbf{I}\|_F}{\sigma^2} \\
&\approx \frac{\|\hat{\mathbf{H}}^* \hat{\mathbf{H}}\|_F}{\sigma^2} \\
&= \frac{\|\hat{\mathbf{H}}\|_F^2}{\sigma^2},
\end{aligned} \tag{57}$$

which is actually the SNR before the LMMSE demodulation. Therefore, we set the SNRs of the  $Q$  received signal copies before demodulation as the weight values and add the corresponding demodulated signals together, which is shown in Fig 4. Each weight value could be calculated as

$$w_{ij} = \frac{|\tilde{\mathbf{s}}_{ij}|^2}{|\tilde{\mathbf{n}}(ij, :)|^2}, \tag{58}$$

where  $1 \leq i \leq P, 1 \leq j \leq Q$ ,  $\tilde{\mathbf{s}} = \hat{\mathbf{H}}\mathbf{s}$ , and  $\tilde{\mathbf{n}} = \mathbf{W}_T^* \mathbf{n}$ . The total weight vector is

$$\mathbf{w} = [\mathbf{w}_1, \mathbf{w}_2, \dots, \mathbf{w}_P], \tag{59}$$

where  $\mathbf{w}_i = [w_{i1}, w_{i2}, \dots, w_{iQ}]$ ,  $i = 1, 2, \dots, P$ , represents the weight vector for the  $i_{th}$  sub-channel and is normalized in advance. The output signal vector is

$$\hat{\mathbf{y}} = [\hat{\mathbf{y}}_1, \hat{\mathbf{y}}_2, \dots, \hat{\mathbf{y}}_P]^T. \tag{60}$$

For each  $\hat{\mathbf{y}}_i, i = 1, 2, \dots, P$ , we have

$$\hat{\mathbf{y}}_i = [\hat{y}_{i1}, \hat{y}_{i2}, \dots, \hat{y}_{iQ}]^T, \tag{61}$$

where each  $\hat{y}_{ij}$  is the linearly combination of the demodulated signals, which could be calculated by

$$\begin{aligned}
\hat{y}_{i1} &= \hat{y}_{i2} = \dots = \hat{y}_{iQ} \\
&= \sum_{j=1}^Q w_{ij} \hat{s}_{ij}.
\end{aligned} \tag{62}$$

In the proposed HYP-SLD-MRC diversity combining scheme, output SNR is maximized for each sub-channel, which could be easily proved by the Chebyshev inequality. For MRC, the diversity gain is proportional to the number of antennas ( $N$ ) since the output SNR is expanded by  $N$  times [32]. Thus, through the proposed HYP-SLD-MRC scheme,  $Q$  times diversity gains

could be obtained which will improve the BER performance. Moreover, we only need to perform diversity combining on each sub-channel, which makes the signals transmitted along different sub-channels independent. Therefore,  $P$  times multiplexing gains could also be obtained.

## V. SIMULATION RESULTS

In this section, we evaluate the performances of the proposed HYP-SLD hybrid precoding scheme and HYP-SLD-MRC diversity combining scheme. We consider a single-user MIMO system and the hybrid system architecture is presented in Fig 1. Both the transmitter and the receiver are equipped with ULA, where the transmitter is equipped with  $N_t = 64$  antennas and  $N_{\text{RF}}^t = 16$  RF chains, and the receiver is equipped with  $N_r = 32$  antennas and  $N_{\text{RF}}^r = 8$  RF chains. According to the measurement activity in downtown Manhattan environment [22]–[24], the frequency of the millimeter wave is set to be 28 GHz and the bandwidth is set to be 100MHz. We adopt the clustered narrow-band millimeter wave channel with sparsity property in the angular domain. For simplicity but without loss of generality, we assume the transmitter and receiver have the same spatial lobe distributions. According to the step procedures for generating the millimeter wave channel in [22], [24], we make some reasonable simplifications and set the channel parameters as follows. For  $P$  spatial lobes, we divide the whole angular domain into  $P$  parts uniformly and the mean angles of spatial lobes ( $\tilde{\theta}_i, i = 1, 2, \dots, P$ ) are uniformly distributed within  $[0, 2\pi]$ , i.e.,  $\tilde{\theta}_i = \frac{2\pi}{P}(i - 1), i = 1, 2, \dots, P$ . The angle spread of each spatial lobe is set as  $\Delta\theta = \frac{\pi}{P}$  to make the angles of paths in different spatial lobes sufficiently separable and the angles of subpaths in one spatial lobe are randomly distributed. The gains of paths in each spatial lobe are assumed to be Rayleigh distributed and the total power of the channel is normalized which satisfies  $\mathbb{E}[\|\mathbf{H}\|_F^2] = N_t N_r$ .

Fig. 5 compares the spectral efficiency of the proposed HYP-SLD, OMP precoding scheme and fully digital precoding scheme (implemented by SVD) with different numbers of spatial lobes. For the millimeter wave channel, the more the number of the spatial lobes is, the more the dominated large singular values become, which will bring higher spectral efficiency. Fig. 5 shows that, the proposed HYP-SLD scheme achieves similar spectral efficiency as the OMP scheme and the fully digital precoding scheme.

In Fig. 6, we present the influence of the number of subpaths on the spectral efficiency. Due to the sparse characteristics of millimeter wave, the number of the subpaths  $Q$  is no more than 4. Different from spatial lobe, the more the number of the subpaths is, the more the relatively

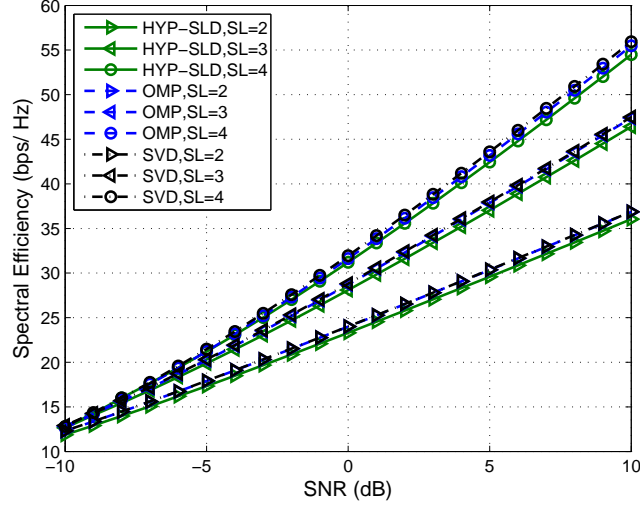


Fig. 5. Spectral efficiencies of HYP-SLD, OMP and fully digital precoding schemes with different numbers of spatial lobes, where  $N_s = PQ$ ,  $N_t = 64$ ,  $N_r = 32$ ,  $N_{\text{RF}}^t = 16$ ,  $N_{\text{RF}}^r = 8$ ,  $Q = 2$ ,  $b = 7$ .

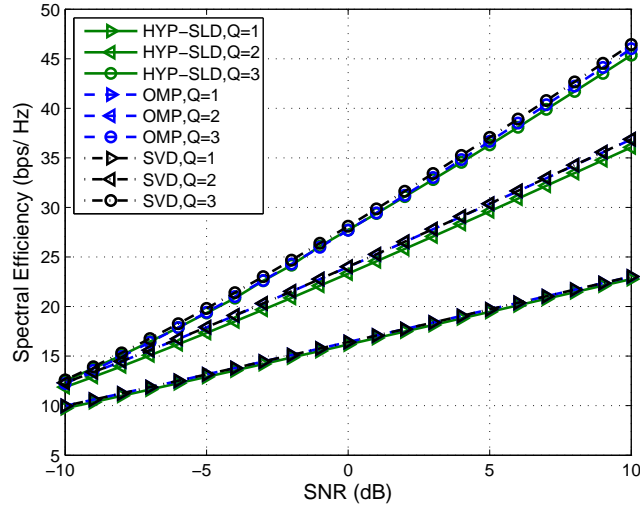


Fig. 6. Spectral efficiencies of HYP-SLD, OMP and fully digital precoding schemes with different  $Q$ , where  $N_s = PQ$ ,  $N_t = 64$ ,  $N_r = 32$ ,  $N_{\text{RF}}^t = 16$ ,  $N_{\text{RF}}^r = 8$ ,  $P = 2$ ,  $b = 7$ .

smaller singular values are, which may contribute relatively less to the spectral efficiency. As we could see in Fig. 6, the spectral efficiency performances of the three schemes are always very close for different numbers of subpaths.

In Fig. 7, the impact of the quantization bit on the spectral efficiency is shown. We observe

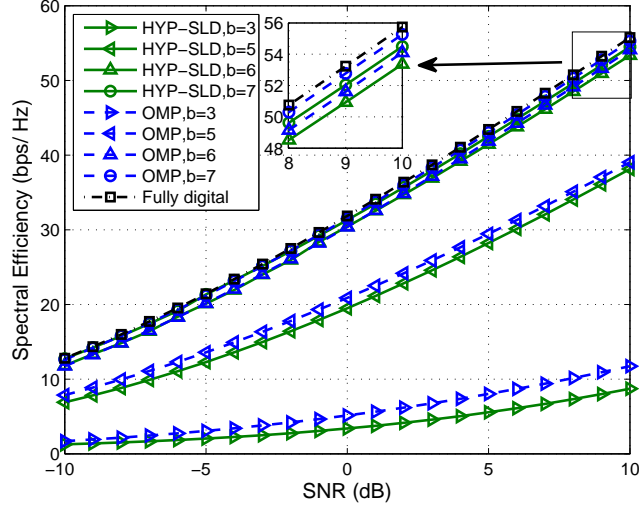


Fig. 7. Spectral efficiencies of HYP-SLD, OMP and fully digital precoding schemes with different quantization bits, where  $N_s = PQ$ ,  $N_t = 64$ ,  $N_r = 32$ ,  $N_{\text{RF}}^t = 16$ ,  $N_{\text{RF}}^r = 8$ ,  $P = 4$ ,  $Q = 2$ .

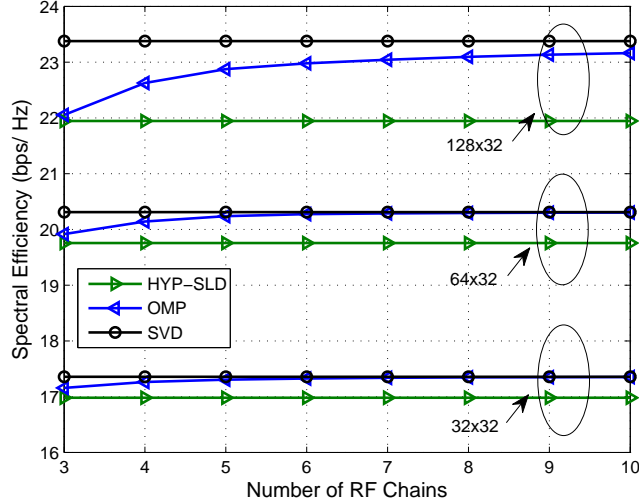


Fig. 8. Spectral efficiencies of HYP-SLD, OMP and fully digital precoding schemes with different numbers of RF chains at the receiver, where  $N_s = PQ$ ,  $\text{SNR} = 0$  dB,  $N_{\text{RF}}^t = N_{\text{RF}}^r$ ,  $P = 1$ ,  $Q = 3$ ,  $b = 7$ .

that when the quantization bit  $b = 6, 7$ , HYP-SLD achieves similar spectral efficiency as the fully digital precoding scheme. However, when  $b=3$  or  $5$ , which satisfies  $2^b < \max(N_t, N_r)$ , the performance of HYP-SLD and OMP schemes decrease. The above results are consistent with the analysis in Section III.B. Generally speaking, the larger the quantization bit is, the better the

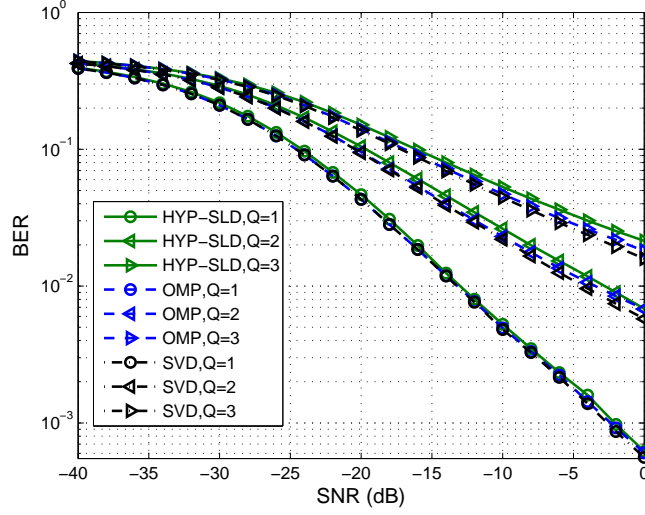


Fig. 9. BERs of HYP-SLD, OMP and fully digital precoding schemes with different  $Q$ , where  $N_s = PQ$ ,  $N_t = 64$ ,  $N_r = 32$ ,  $N_{\text{RF}}^t = 16$ ,  $N_{\text{RF}}^r = 8$ ,  $P = 2$ .

performance becomes. However, the complexity will also increase dramatically with the increase of  $b$ . In the meantime, we could see that the spectral efficiencies for  $b = 6$  and  $b = 7$  are very close. Therefore, when the quantization bit  $b$  is large enough, the performance will not increase too much with the increase of the quantization bit.

Fig. 8 shows the spectral efficiencies of different schemes with different numbers of RF chains at the receiver, where the SNR is set to be 0 dB. We observe that when  $N_{\text{RF}}^r$  varies from 2 to 10, the spectral efficiencies of HYP-SLD remain unchanged. The performance gap originates from two main aspects. 1) We utilize the array response matrices as the reference matrices instead of the optimal precoding matrices; 2) We only utilize  $N_{\text{RF}}^r = N_{\text{RF}}^t = PQ$  RF chains to transmit and receive signals. Note that, the performance gaps are no more than 5% while the complexity could be reduced by 99%.

In Fig. 9 and Fig. 10, we compare the BER performances of HYP-SLD, OMP and the fully digital precoding schemes with different numbers of the subpaths and spatial lobes, respectively. The modulation scheme is QPSK. We observe that the three schemes achieve nearly the BER performances for different  $Q$  and  $P$ . Moreover, the BER performances for different numbers of spatial lobes are very close. However, when the number of the subpaths increases, the BER performances decreases greatly. The above phenomenon demonstrates that the number of subpaths has a greater impact on the BER performance.

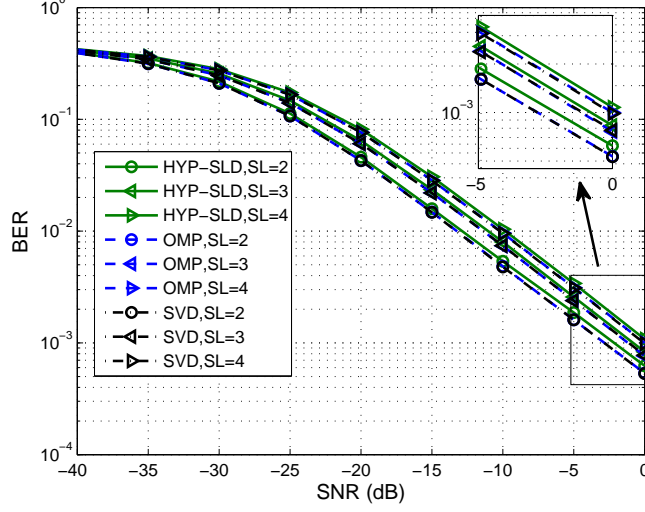


Fig. 10. BERs of HYP-SLD, OMP and fully digital precoding schemes with different numbers of spatial lobes, where  $N_s = PQ$ ,  $N_t = 64$ ,  $N_r = 32$ ,  $N_{\text{RF}}^t = 16$ ,  $N_{\text{RF}}^r = 8$ ,  $Q = 1$ .

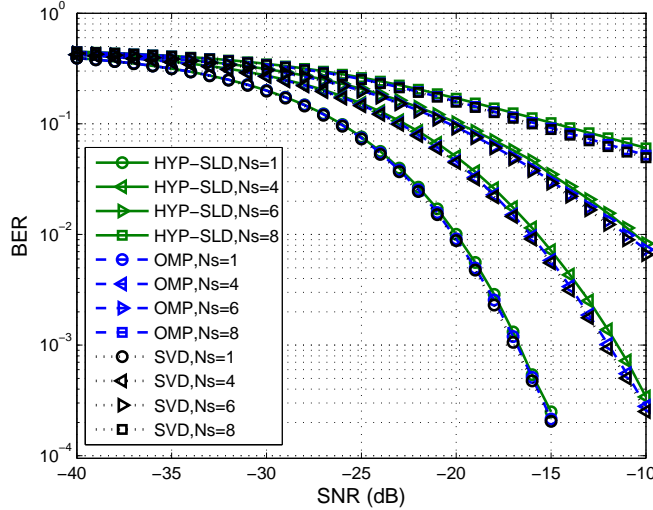


Fig. 11. BERs of HYP-SLD, OMP and fully digital precoding schemes with different numbers of data streams, where  $N_t = 64$ ,  $N_r = 32$ ,  $N_{\text{RF}}^t = 16$ ,  $N_{\text{RF}}^r = 8$ ,  $P = 4$ ,  $Q = 2$ .

In Fig. 11, we compare the BER performances of the proposed HYP-SLD, OMP and the fully digital precoding with different numbers of data streams, where the number of the spatial lobe is set to be 4, and the number of the subpaths is set to be 2. Note that, we always keep the number of the data streams equal to the number of paths at the transmitter. After SVD for

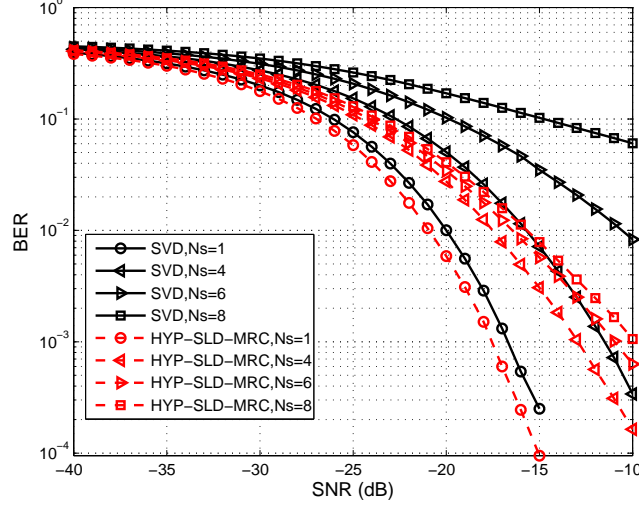


Fig. 12. BERs of the proposed HYP-SLD-MRC and the fully digital precoding schemes with different numbers of data streams, where  $N_t = 64$ ,  $N_r = 32$ ,  $N_{\text{RF}}^t = 16$ ,  $N_{\text{RF}}^r = 8$ ,  $P = 4$ ,  $Q = 2$ .

each sub-channel, we select data streams corresponding to the  $N_s$  largest singular values at the receiver. As we could see In Fig. 11, when  $N_s$  varies from 1 to 8, the BER performances of the three precoding schemes are almost the same.

Fig. 12 shows the BER performances of the proposed HYP-SLD-MRC diversity combining scheme and the fully digital precoding scheme, where the number of the spatial lobes is 4 and the number of the subpaths is 2. It could be observed that the BER performances of HYP-SLD-MRC always outperform the fully digital precoding for different numbers of data streams. Moreover, the more the number of data streams is, the more obvious the performance improvement becomes. This is because smaller singular values are used to transmit signals when the number of data streams becomes larger. The proposed HYP-SLD-MRC is able to transmit the signal copy along the smallest singular value and achieves the maximum output SNR for each sub-channel.

## VI. CONCLUSIONS

In this paper, we proposed a low complexity hybrid analog/digital precoding scheme and a diversity combining scheme in the millimeter wave MIMO systems. We fully utilize the sparseness property in the angular domain of the millimeter wave to design the low complexity hybrid precoding scheme. Compared with the widely used OMP scheme, the proposed HYP-SLD reduces the complexity more than 99%. To improve the BER performance, we proposed a new

type of diversity combining scheme to maximize the output SNR for each sub-channel, which allows the diversity gains and the multiplexing gains to be obtained at the same time. Simulation results have demonstrated that the proposed low complexity hybrid precoding scheme exhibits similar spectral efficiency and BER performances as the fully digital precoding scheme. Moreover, the proposed HYP-SLD-MRC achieves more than 5dB improvement in BER performance compared with the fully digital precoding scheme.

## REFERENCES

- [1] T. S. Rappaport, S. Sun, R. Mayzus, H. Zhao, Y. Azar, K. Wang, G. N. Wong, J. K. Schulz, M. Samimi, and F. Gutierrez, "Millimeter wave mobile communications for 5G cellular: It will work!" *IEEE Access*, vol. 1, pp. 335-349, May 2013.
- [2] "Wireless HD specification overview," Tech. Rep., 2010 [Online]. Available: <http://www.wirelesshd.org/pdfs/WirelessHD-Specification-Overview-v1.1May2010.pdf>
- [3] ISO/IEC/IEEE International Standard for Information Technology-Telecommunications and Information Exchange Between Systems-Local and Metropolitan Area Networks-Specific Requirements-Part 11: Wireless LAN Medium Access Control (MAC) and Physical Layer (PHY) Specifications Amendment 3: Enhancements for Very High Throughput in the 60 GHz Band (adoption of IEEE Std 802.11ad-2012), ISO/IEC/IEEE 8802C11:2012/Amd.3:2014(E), Mar. 2014, pp. 1-634.
- [4] R. W. Heath, N. Gonzalez-Prelcic, S. Rangan, W. Roh and A. M. Sayeed, "An overview of signal processing techniques for millimeter wave MIMO systems," *IEEE J. Sel. Areas Commun.*, vol. 10, no. 3, pp. 436-453, Apr. 2016.
- [5] C. X. Wang, F. Haider, X. Gao, X. H. You, Y. Yang, D. Yuan, H. M. Aggoune, H. Haas, S. Fletcher, and E. Hepsaydir, "Cellular architecture and key technologies for 5G wireless communication networks," *IEEE Commun. Mag.*, vol. 52, no. 2, pp. 122-130, Feb. 2014.
- [6] S. Rangan, T. S. Rappaport, and E. Erkip, "Millimeter-wave cellular wireless networks: Potentials and challenges," *Proc. IEEE*, vol. 102, no. 3, pp. 366-385, Mar. 2014.
- [7] Y. Wu, C. Xiao, Z. Ding, X. Gao and S. Jin, "Linear precoding for finite-alphabet signaling over MIMOME wiretap channels," *IEEE Trans. Veh. Technol.*, vol. 61, no. 6, pp. 2599-2612, Jul. 2012.
- [8] D. P. Palomar, J. M. Cioffi and M. A. Lagunas, "Joint Tx-Rx beamforming design for multicarrier MIMO channels: a unified framework for convex optimization," *IEEE Trans. Signal Process.*, vol. 51, no. 9, pp. 2381-2401, Sep. 2003.
- [9] Z. Pi and F. Khan, "An introduction to millimeter-wave mobile broadband systems," *IEEE Commun. Mag.*, vol. 49, no. 6, pp. 101-107, Jun. 2011.
- [10] J. Wang, "Beam codebook based beamforming protocol for multi-Gbps millimeter-wave WPAN systems," *IEEE J. Sel. Areas Commun.*, vol. 27, no. 8, pp. 1390-1399, Oct. 2009.
- [11] X. Zhang, A. Molisch, and S. Kung, "Variable-phase-shift-based RF-baseband codesign for MIMO antenna selection," *IEEE Trans. Signal Process.*, vol. 53, no. 11, pp. 4091-4103, Nov. 2005.
- [12] V. Venkateswaran and A. van der Veen, "Analog beamforming in MIMO communications with phase shift networks and online channel estimation," *IEEE Trans. Signal Process.*, vol. 58, no. 8, pp. 4131-4143, Aug. 2010.
- [13] O. E. Ayach, S. Rajagopal, S. Abu-Surra, Z. Pi, and R. W. Heath, Jr, "Spatially sparse precoding in millimeter wave MIMO systems," *IEEE Trans. Wireless Commun.*, vol. 13, no. 3, pp. 1499-1513, Mar. 2014.
- [14] A. Alkhateeb, O. El Ayach, G. Leus, and R. W. Heath, Jr, "Hybrid precoding for millimeter wave cellular systems with partial channel knowledge," in *Proc. Inf. Theory Applicat. Workshop*, San Diego, CA, USA, Feb. 2013, pp. 1-5.

- [15] C. Rusu, R. Mndez-Rial, N. Gonzlez-Prelcic and R. W. Heath, "Low complexity hybrid precoding strategies for millimeter wave communication systems," *IEEE Trans. Wireless Commun.*, vol. 15, no. 12, pp. 8380-8393, Dec. 2016.
- [16] J. Singh and S. Ramakrishna, "On the feasibility of codebook-based beamforming in millimeter wave systems with multiple antenna arrays," *IEEE Trans. Wireless Commun.*, vol. 14, no. 5, pp. 2670-2683, May 2015.
- [17] S. Park, A. Alkhateeb and R. W. Heath, "Dynamic subarrays for hybrid precoding in wideband mmWave MIMO systems," *IEEE Trans. Wireless Commun.*, vol. 16, no. 5, pp. 2907-2920, May 2017.
- [18] Y. Y. Lee, C. H. Wang, and Y. H. Huang, "A Hybrid RF/baseband precoding processor based on parallel-index-selection matrix-inversion-bypass simultaneous orthogonal matching pursuit for millimeter wave MIMO systems," *IEEE Trans. Signal Process.*, vol. 63, no. 2, pp. 305-317, Jan. 2015.
- [19] C. H. Chen, C. R. Tsai, Y. H. Liu, W. L. Hung and A. Y. Wu, "Compressive sensing (CS) assisted low-complexity beamspace hybrid precoding for millimeter-wave mimo systems," *IEEE Trans. Signal Process.*, vol. 65, no. 6, pp. 1412-1424, Mar. 2017.
- [20] Y. Zeng and R. Zhang, "Millimeter wave MIMO with lens antenna array: A new path division multiplexing paradigm," *IEEE Trans. Commun.*, vol. 64, no. 4, pp. 1557-1571, Apr. 2016.
- [21] Y. Zeng, and R. Zhang, "Cost-effective millimeter wave communications with lens antenna array", *IEEE Wireless Commun.*, vol. 24, no. 4, pp. 81-87, Aug. 2017.
- [22] M. K. Samimi and T. S. Rappaport, "Ultra-wideband statistical channel model for non line of sight millimeter-wave urban channels," in *Proc. IEEE Global Commun. Conf.*, Austin, TX, Dec. 2014, pp. 3483-3489.
- [23] M. K. Samimi and T. S. Rappaport, "3-D millimeter-wave statistical channel model for 5G wireless system design," *IEEE Trans. Microw. Theory Techn.*, vol. 64, no. 7, pp. 2207-2225, Jul. 2016.
- [24] T. S. Rappaport, G. R. MacCartney, M. K. Samimi, and S. Sun, "Wideband millimeter-wave propagation measurements and channel models for future wireless communication system design," *IEEE Trans. Commun.*, vol. 63, no. 9, pp. 3029-3056, Sep. 2015.
- [25] A. Alkhateeb, O. El Ayach, G. Leus, and R. W. Heath, "Channel estimation and hybrid precoding for millimeter wave cellular systems," *IEEE J. Sel. Topics Signal Process.*, vol. 8, no. 5, pp. 831-846, Oct. 2014.
- [26] A. Goldsmith, S. Jafar, N. Jindal, and S. Vishwanath, "Capacity limits of MIMO channels," *IEEE J. Sel. Areas Commun.*, vol. 21, no. 5, pp. 684-702, 2003.
- [27] O. El Ayach, R. Heath, S. Abu-surra, S. Rajagopal, and Z. Pi, "The capacity optimality of beam steering in large millimeter wave MIMO systems," in *Proc. IEEE 13th Int. Workshop Signal Process. Adv. Wireless Commun.*, Jun. 2012, pp. 100-104.
- [28] D. Tse and P. Viswanath, *Fundamentals of Wireless Communication*. New York, USA: Cambridge University Press.
- [29] Y. P. Lin, "On the quantization of phase shifters for hybrid precoding systems," *IEEE Trans. Signal Process.*, vol. 65, no. 9, pp. 2237-2246, May 2017.
- [30] Y. Han, H. Zhang, S. Jin, X. Li, R. Yu and Y. Zhang, "Investigation of transmission schemes for millimeter-wave massive MU-MIMO systems," *IEEE Syst. J.*, vol. 11, no. 1, pp. 72-83, Mar. 2017.
- [31] M. Z. Win and J. H. Winters, "Analysis of hybrid selection/maximal-ratio combining in Rayleigh fading," *IEEE Trans. Commun.*, vol. 47, no. 12, pp. 1773-1776, Dec. 1999.
- [32] D. G. Brennan, "Linear diversity combining techniques," *Proc. IRE*, vol. 47, no. 6, pp. 1075-1102, Jun. 1959.